

QUASI-PERIODIC X-RAY FLARES FROM THE PROTO STAR YLW 15

Yohko Tsuboi¹, Kensuke Imanishi and Katsuji Koyama²Department of Physics, Faculty of Science, Kyoto University, Sakyo-ku, Kyoto 606-8502, Japan
tsuboi@cr.scp.phys.kyoto-u.ac.jp, kensuke@cr.scp.phys.kyoto-u.ac.jp, koyama@cr.scp.phys.kyoto-u.ac.jp

and

Nicolas Grosso and Thierry Montmerle

Service d'Astrophysique, CEA/DAPNIA/SAp, Centre d'Etudes de Saclay, 91191 Gif-sur-Yvette Cedex,
France
gross@discovery.saclay.cea.fr, montmerle@discovery.saclay.cea.fr

To be submitted to ApJ

ABSTRACT

With ASCA, we have detected three X-ray flares from the Class I protostar YLW 15. The flares occurred every 20 hours and showed an exponential decay with time constant 30{60 ks. The X-ray spectra are explained by a thin thermal plasma emission. The plasma temperature shows a fast-rise and slow-decay for each flare with $kT_{\text{peak}} = 4.6 \text{ keV}$. The emission measure of the plasma shows this time profile only for the first flare, and remains almost constant during the second and third flares at the level of the tail of the first flare. The peak flare luminosities $L_{\text{X,peak}}$ were $5\{20 \times 10^{31} \text{ erg s}^{-1}$, which are among the brightest X-ray luminosities observed to date for Class I protostars. The total energy released in each flare was $3\{6 \times 10^{36} \text{ ergs}$. The first flare is well reproduced by the quasi-static cooling model, which is based on solar flares, and it suggests that the plasma cools mainly radiatively, confined by a semi-circular magnetic loop of length $14R$ with diameter-to-length ratio 0.07 . The two subsequent flares were consistent with the reheating of the same magnetic structure as of the first flare. The large-scale magnetic structure and the periodicity of the flares imply that the reheating events of the same magnetic loop originate in an interaction between the star and the disk due to the differential rotation.

Subject headings: stars: flares | stars: formation | stars: individual (IRAS 43, YLW 15) | stars: late-type | X-rays: spectra | X-rays: stars

1. INTRODUCTION

Low-mass Young Stellar Objects (YSOs) evolve from molecular cloud cores through the protostellar (ages $10^4\text{--}5$ yr), the Classical T Tauri (CTTS: 10^6 yr) and Weak-lined T Tauri (WTTS: 10^7 yr) phases to main sequence. Protostars are generally associated with the Class 0 and I spectral energy distributions (SEDs), which peak respectively in the millimeter and infrared (IR) bands. Bipolar flows are accompanied with this phase, suggesting dynamical gas accretion. CTTSs have still circumstellar disks though they have expelled or accreted the infalling envelopes. They are associated with the Class II spectra, which peak at the near-IR. Finally, as the circumstellar disk disappears, YSOs evolve to WTTSs, associated with Class III stars. Early stellar evolution is reviewed by Shu, Adams, & Lizano (1987) and Andre & Montmerle (1994).

The Einstein Observatory discovered that T Tauri Stars (TTSs), or Class II and Class III infrared objects, are strong X-ray emitters, with the luminosities of $100\{10000$ times larger than solar flares. These X-rays showed high amplitude time variability like solar flares. The temperature (1 keV) and plasma density ($n_e = 10^{11} \text{ cm}^{-3}$) are comparable to those of the Sun, hence the X-ray emission mechanism has been thought to be a scaled-up version of solar X-ray emission; i.e., magnetic activity on the stellar surface enhanced by a dynamo process (Feigelson & De-

Campli 1981; Montmerle et al. 1983). X-ray and other high energy processes in YSOs are reviewed by Feigelson & Montmerle (1999).

In contrast to TTSs, Class I infrared objects are generally surrounded by circumstellar envelopes of A_V up to 40 or more, hence are almost invisible in the optical, near infrared and even soft X-ray bands. The ASCA satellite, sensitive to high energy X-rays up to 10 keV which can penetrate heavy absorption, has found X-rays from Class I objects in the cores of the R CrA, Oph, and Orion clouds at the hard band ($> 2 \text{ keV}$) (Koyama et al. 1994; Koyama et al. 1996; Kamata et al. 1997, Ozawa et al. 1999). Even in the soft X-ray band, deep exposures with the ROSAT Observatory detected X-rays from YLW 15 in Oph (Grosso et al. 1997) and CrA (Neuhäuser & Preibisch 1997).

A notable aspect of these pioneering observations was the discovery of X-ray flares from Class I stars. ROSAT discovered a giant flare from the protostar YLW 15 with total luminosity (over the full X-ray band) of $10^{34}\text{--}36 \text{ erg s}^{-1}$, depending on the absorption. ASCA observed more details of X-ray flares from protostars EL29 in the Ophiuchus, R1 in the R CrA core, and SSV 63E+W in the Orion, which are associated with larger $N_H = 10^{22}\text{--}23 \text{ cm}^{-2}$ than seen in TTSs.

All these findings led us to deduce that greatly enhanced

¹Present address: Department of Astronomy & Astrophysics, The Pennsylvania State University, University Park, PA 16802-6305, USA

²CREST, Japan Science and Technology Corporation (JST), 4-1-8 Honmachi, Kawaguchi, Saitama 332-0012, Japan

magnetic activity, already well-established in older TTSSs, is present in the earlier protostellar phase. Stimulated by these results, and to search for further examples of the protostellar activity in the X-ray band, we have performed an extensive follow-up observation of a core region in Oph, with several Class I X-ray sources. The follow-up observation was made with ASCA 3.5 years after the first observation (Koyama et al. 1994, Kamata et al. 1997). Some previously bright Class Is became dim, while other Class Is were identified as hard X-ray sources. This paper discusses the brightest hard X-ray source, Y LW 15, concentrating on the characteristics and implications of its peculiar time behavior: quasi-periodic hard X-ray flares. For comparison with previous results, we assume the distance to the Oph region to be 165 pc (Dame et al. 1987) throughout this paper, although new Hipparcos data suggest a closer distance of 120 pc (Knude & Hog 1998).

2. OBSERVATION

We observed the central region of Oph cloud with ASCA for 100 ks on 1997 March 23. The telescope pointing coordinates were (2000) = 16h 27.4m and (2000) = 24° 30'. All four detectors, the two Solid-state Imaging Spectrometers (SIS 0, SIS 1) and the two Gas Imaging Spectrometers (GIS 2, GIS 3) were operating in parallel, providing four independent data sets. Details of the instruments, telescope and detectors are given by Burke et al. (1991), Tanaka, Inoue, & Holt (1994), Serlemitsos et al. (1995), Ohashi et al. (1996), Makishima et al. (1996), and Gotthelf (1996).

Each of the GIS was operated in the Pulse Height mode with the standard bit assignment that provides time resolutions of 62.5 ms and 0.5 s for high and medium bit rates, respectively. The data were post-processed to correct for the spatial gain non-linearity. Data taken at geomagnetic rigidities lower than 6 GV, at elevation angles less than 5° from the Earth, and during passage through the South Atlantic Anomaly were rejected. After applying these filters, the net observing time for both GIS 2 and GIS 3 was 94 ks.

Each of the SIS was operated in the 4-CCD/Faint mode (high bit rate) and in the 2-CCD/Faint mode (medium bit rate). However, we concentrate on the 4-CCD/Faint results in this paper since Y LW 15 is out of the 2-CCD field of view. The data were corrected for spatial and gain non-linearity, residual dark distribution, dark frame error, and hot and flickering CCD pixels using standard procedures. Data were rejected during South Atlantic Anomaly and low elevation angles as with GIS data. In order to avoid contamination due to light leaks through the optical blocking filters, we excluded data taken when the satellite viewing direction was within 20° of the bright rim of the Earth. After applying these filters, the net observing time for the 4-CCD mode was 61 ks for SIS 0 and 63 ks for SIS 1.

Towards the end of this observation, we detected an enormous flare from T Tauri star ROX s31 which is located close to Y LW 15 (see x3.1, source 6 in Figure 1). The peak flux of ROX s31 is 1.2 orders of magnitude larger than Y LW 15 (see x4.2), and its broad point spread function contaminates Y LW 15 during the flare. Therefore, we excluded the GIS and SIS data taken during the flare of ROX s31 in all analysis of Y LW 15.

3. RESULTS AND ANALYSIS

3.1. Images

Figure 1 shows X-ray images of the Ophiuchi Core F region in the two different energy bands (left panel: 0.7-2 keV, right panel: 2-10 keV), obtained with SIS detectors. Class I sources are indicated by crosses. Since the absolute ASCA positional errors can be as large as 40° for SISs (Gotthelf 1996), we compared the ASCA peak positions to the more accurately known IR positions of two bright sources in the SIS field, ROX s21 (source 5) and ROX s31 (source 6), which are indicated by filled circles in Figure 1 left panel. To obtain the ASCA peak positions, we executed a two-dimensional fitting in the 0.7-2 keV band; we fitted these sources with a position-dependent point spread function in the 0.7-2 keV band and a background model. This procedure was done in the Display45 analysis software package (Ishisaki et al. 1998). The position of ROX s31 was based on the flare phase of this source, while the position of ROX s21 is based on the data before the flare of ROX s31. IR positions are provided by Barsony et al. (1997). The ASCA SIS positions had an average offset (weighted mean by photon counts) of +0.18 s in right ascension and 7.4° in declination from the IR frame. This positional offset is corrected in Figure 1. After the bore-sight error correction, remaining excursions between the X-ray and IR positions are 5.5° (rms), which is consistent with the SIS position uncertainty for point sources (Gotthelf 1996). We take the systematic positional error to be 5.5°.

From the 2-10 keV band image, we find that the X-ray fluxes from Class I protostars EL29 and WL6 (sources 3 and 4 in Figure 1, right panel) are fainter by one third and less than one third, respectively, comparing to those in the first ASCA observation made in August 1993 (Kamata et al. 1997). The brightest X-ray source in the 2-10 keV band is an unresolved source at (2000) = 16h 27m 27.0s and (2000) = 24° 40' 50'' in the position corrected frame. We derived this peak position by the two-dimensional fitting in 2-10 keV band. Since the statistical error is 1°, the overall X-ray error (including the systematic error) is 6°.

The closest IR source is Y LW 15 with VLA position of (2000) = 16h 27m 26.9s and (2000) = 24° 40' 49.8'' (0.5°; Leous et al. 1991), located 1.5° away from the X-ray source. The next nearest source is GY 263 with IR position of (2000) = 16h 27m 26.6s and (2000) = 24° 40' 44.9'' (1.3°; Barsony et al. 1997). The source is located 5.5° from the X-ray position on the border of the X-ray position error circle. Thus we conclude that the hard X-rays are most likely due to the Class I source Y LW 15.

3.2. X-ray Lightcurve of Y LW 15

We extracted a lightcurve from a 3° radius circle around the X-ray peak of Y LW 15 (see Figure 1). Before the enormous flare from T Tauri star ROX s31, which occurred in the last phase of this observation (see x2), we detected another large flare from Class II source SR 24N, located about 7° away from Y LW 15 in the GIS field of view. To subtract the time variable contamination from the SR 24N in the extended flux of Y LW 15, we selected a 3° radius back-

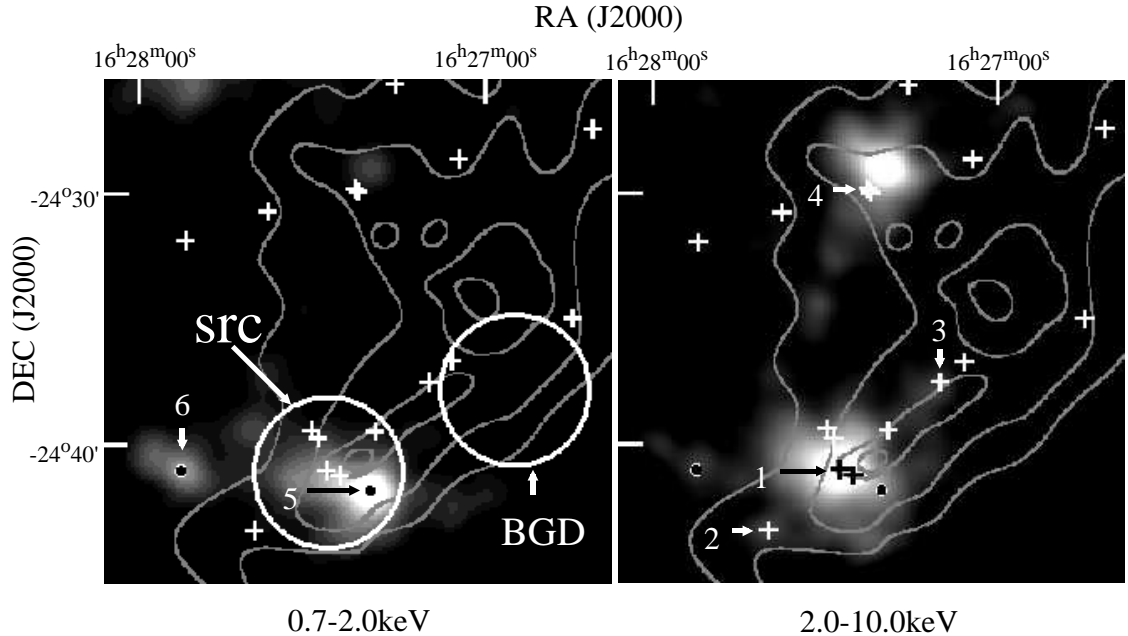


Fig. 1. The SIS images of the central region of Oph cloud in the 0.7-2 keV (left) and the 2-10 keV band (right). The contours are C¹⁸O (1-10) column densities (Wilking & Lada 1983) in units of 10¹⁶ cm⁻², from 1.0 to 2.5 in steps of 0.5, corresponding to A_V = 30, 50, 70, 100, respectively. Class I sources are indicated by crosses (Chen et al. 1995, 1997; Motte, Andre, & Neri 1998). The bright sources 5 and 6 in the 0.7-2 keV band are T Tauri star ROX s21 and ROX s31, respectively. In the 2-10 keV band in age, the brightest source is Class I source Y LW 15 (source 1). Two older Class I sources, IR S51 (source 2) and EL29 (source 3), which have flat SEDs are also detected with a criterion of S/N = 5. EL29 and W L6 (source 4) are faint, though both of them emitted strong X-rays in the first ASCA observation (Koyama et al. 1994; Kamata et al. 1997). The hard X-ray source near W L6 is a cluster of T Tauri stars (W L3, W L4, W L5; Wilking & Lada 1983). The source region and background region for Y LW 15 are also shown by circles.

ground region (see Figure 1), equidistant from SR 24N and Y LW 15. On the other hand, using such a background, we cannot exclude the contamination from ROX s21 (source 5 in Figure 1), which is 2 arcmin apart from Y LW 15. Since the X-rays from ROX s21 are dominant below 2 keV (see x3.3 and Fig. 3), we examine the time variability only in the hard X-ray band (> 2 keV) in which the flux is dominated by Y LW 15.

Figure 2 (upper panel) shows the background-subtracted lightcurve in the 2-10 keV band with the sum of the SIS (SIS 0 and 1) and GIS (GIS 2 and 3) images. The lightcurve shows a saw tooth pattern with three areas. The peak fluxes of the areas become successively less luminous. Each area exhibits a fast rise and an exponential decay with an e-folding time of 31.1 ks ($\tau = \ln 2 / \alpha = 61/46$), 33.3 ks (80/47), and 58⁺²⁴₋₁₃ ks (33/24), for the first, the second, and the third areas, respectively. We show the best-fit lightcurves for the second and the third areas with dashed lines, and show the best-fit quasi-static model (see x4.1.1) for the first area with a solid line in Figure 2 upper panel.

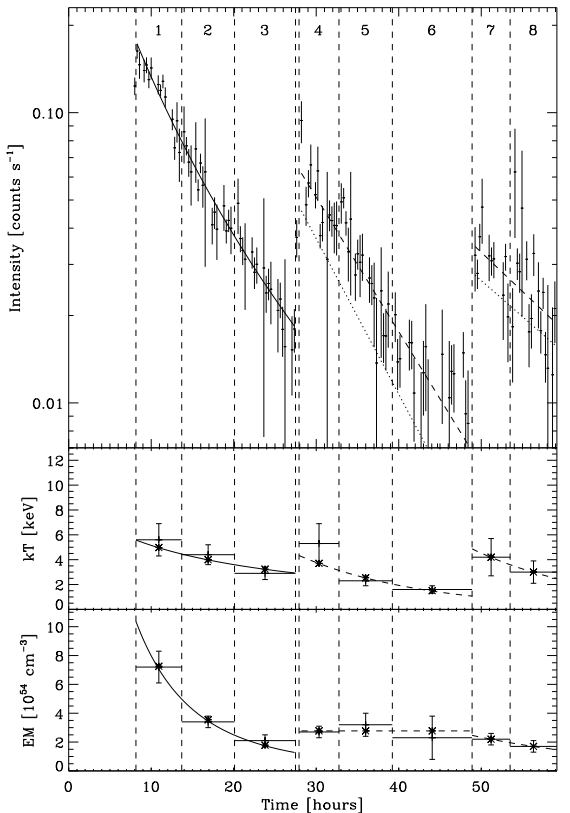


Fig. 2.] Upper panel: Background-subtracted lightcurve of Y LW 15 obtained with all the detectors (SIS 0 + SIS 1 + GIS 2 + GIS 3) in the 2–10 keV band. All time bins are 1024 s wide. Middle panel: Time profile of the best-fit temperature. The error bars indicate 90% confidence. Lower panel: Same as the middle panel, but for the best-fit emission measure. The solid lines during Flare I are the best-fit quasi-static model, and the dashed lines during Flare II and III are the best-fit exponential model (see Table 2). One reheating plasma loop is assumed in both cases. Dotted lines during Flare II and III in the upper panel show each flare component without the contribution of the other flares, under assumption that the three flares occurred independently (see x3.1). A asterisks show the average of the model during one time bin. The time axis starts at 00:00:00.0 UT (1997 March 2).

3.3. Time-Sliced Spectra of Y LW 15

To investigate the origin of the quasi-periodic flares, we made time-sliced spectra for the time intervals given in Figure 2. We extracted the source and background data for each phase from the same regions as those in the lightcurve analysis (see x3.2 and Figure 1). We found that all the spectra show a local flux minimum at 1.2 keV. For example, we show the spectra obtained with SISs at phases 1 and 8 in Figure 3. This suggests that the spectra have two components, one hot and heavily absorbed, the other cool and less absorbed.

Then we examined possible contamination from the bright, soft X-ray source ROX s21 (source 5 in Figure 1). We extracted the spectrum of ROX s21 from a 2^0 radius circle around its X-ray peak. We extracted the data only during phase 1, in order to be free from contamination from the flare on SR 24N, which occurred during phases 4–6 (see x3.2). The background data for ROX s21 were extracted from a 2^0 radius circle equidistant from Y LW 15 and ROX s21 during phase 1. After the subtraction of the background, the spectrum of ROX s21 is well reproduced by an optically thin thermal plasma model of about 0.6 keV temperature with absorption fixed at $N_H = 1.3 \times 10^{21}$ cm $^{-2}$ ($A_V = 0.6$ mag; Bouvier and Appenzeller 1992) with $\chi^2/\text{d.o.f.} = 17/23$. The flux of the soft component of Y LW 15 is about 30% of the flux of ROX s21, which is equal to the spill-over flux from ROX s21. Thus the soft X-ray component found in Y LW 15 spectra is due to contamination from the nearby bright source ROX s21.

Having obtained the best-fit spectrum for ROX s21, we fitted the spectrum of Y LW 15 in each phase with a two-temperature thermal plasma model. The cool component is set to the contamination from ROX s21, and the hot component is from Y LW 15. For Y LW 15, free parameters are temperature (kT), emission measure (EM), absorption (N_H) and metal abundance. For ROX s21, EM is the only free parameter and the other parameters are fixed to the best-fit values obtained in phase 1. We found no significant variation in N_H of Y LW 15 from phase to phase, hence, we fixed the N_H to the best-fit value at phase 1. The resulting best-fit parameters of Y LW 15 for each time interval are shown in Table 1. The best-fit spectra of phases 1 and 8 are illustrated in Figure 3, and the time evolution of the best-fit parameters are shown in Figure 2.

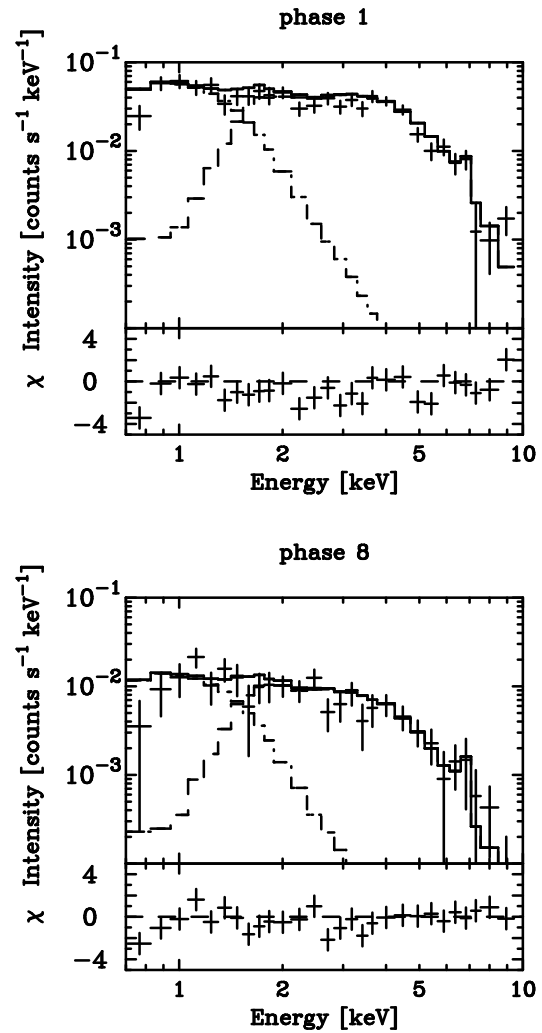


Fig. 3.] The SIS (SIS 0 + 1) spectra of Y LW 15 at phase 1 and 8 (see Figure 2). The solid lines show the best-fit two-temperature coronal plasma model derived from simultaneous fitting of GIS and SIS data. Lower panel shows the residuals from the best-fit model.

4. DISCUSSION

In this observation, we detected hard X-rays (> 2 keV) from the Class I source Y LW 15 for the first time; the source was not detected in the first ASCA observation executed 3.5 years later (Kamata et al. 1997). On the other hand, the Class I sources EL29 and WL6, which emitted bright hard X-rays in the first observation, became very faint (see x3.1). Then we conclude that hard X-rays from Class I protostars in the Oph cloud are highly variable in the time spans, and we suspect that the non-detection of hard X-rays from other Class I objects is partly due to the long-term time variability. From Y LW 15, we discovered a peculiar time behavior: quasi-periodic flares. We shall now discuss the relation between each flare from Y LW 15 and the physical conditions.

4.1. Physical Parameters of the Triple Flare

If the three intermittent flares are attributed to a single persistent flare, with the three events due to geometrical modulation, such as occultation of the flaring region by

Table 1
Best-fit parameters to the spectra of Y LW 15^a.

Phase ^b	kT (keV)	Abundance (solar)	EM ^c (10^{54} cm^{-3})	L_X^d ($10^{31} \text{ erg s}^{-1}$)	$\chi^2/\text{d.o.f}$
1	$5.6^{+1.3}_{-1.0}$	$0.4^{+0.2}_{-0.1}$	$7.2^{+1.1}_{-0.8}$	15 1	181/106
2	$4.4^{+0.8}_{-0.7}$	$0.4^{+0.2}_{-0.2}$	$3.4^{+0.4}_{-0.3}$	6.0 0.7	191/164
3	$2.9^{+0.5}_{-0.3}$	$0.7^{+0.5}_{-0.4}$	$2.1^{+0.4}_{-0.3}$	3.4 0.8	80/84
4	$5.3^{+1.6}_{-1.1}$	$0.6^{+0.4}_{-0.4}$	$2.7^{+0.4}_{-0.3}$	5.6 0.8	55/52
5	$2.3^{+0.4}_{-0.3}$	$0.5^{+0.6}_{-0.4}$	$3.2^{+0.8}_{-0.7}$	4.4 1.3	163/138
6	$1.6^{+0.3}_{-0.3}$	< 1.3	$2.3^{+1.5}_{-1.2}$	2.5 1.5	46/40
7	$4.2^{+1.5}_{-0.9}$	< 0.4	$2.2^{+0.4}_{-0.3}$	3.5 0.5	153/139
8	$3.0^{+0.9}_{-0.5}$	$0.7^{+1.3}_{-0.5}$	$1.7^{+0.4}_{-0.4}$	2.9 0.6	59/65

Note. | The errors are at 90% confidence level.

^a Absorption column density is fixed to the best fit value for phase 1, $3.3 \times 10^{22} \text{ cm}^{-2}$.

^b see Figure 2.

R

^c Emission measure, $n_e^2 dV$ (n_e : electron density, V : emitting volume).

^d Absorption-corrected X-ray luminosity in the 0.1 - 100 keV band.

stellar rotation or orbit in an inner disk, then only the emission measure should have shown three peaks. The temperature would have smoothly decreased during the three arcs. However, in our case, we see the temperature following the same pattern as the luminosity, decreasing after each jump, as indicated in Table 1 and Figure 2 middle panel. To test further, we fitted the temperatures in phases 1-8 with a single exponential decay model, and concluded that it is rejected with 89% confidence. We then interpret the variability of Y LW 15 as due to a triple arc, in which each arc is followed by a cooling phase. Now, let us label phases 1-3, 4-6, and 7-8 as Flare I, II, and III, respectively. In this subsection we will use the cooling phases to estimate the physical conditions of the plasma in each arc. Details are given in the Appendix.

4.1.1. Flare I

Here we assume that the plasma responsible for Flare I is confined in one semi-circular magnetic loop with constant cross section along the tube axis, with length L , and diameter-to-length (aspect) ratio a , based on the general analogy of solar-type arcs. To the decay of Flare I, we apply a quasi-static cooling model (van den Oord & Mewe 1989), in which the hot plasma cools quasi-statically as a result of radiative (90%) and conductive (10%) losses (see detailed comment in Appendix x1). If the cooling is truly quasi-static, $T^{13=4} = EM$ shows constant during the decay (where T is plasma temperature and EM is the emission measure). We find for the three successive bins (phases 1-3) of Flare I that $(T=10^7 \text{ K})^{13=4} = (EM=10^{54} \text{ cm}^{-3}) = 61, 55, 59, 42, 25, 18$, which are not inconsistent with a constant value, taking into account the large error bars. Then, fitting our data with the quasi-static model, we find satisfactory values of χ^2_{red} for the count rates, temperature, and emission measure (see panel 1 in Table 2). We conclude that our hypothesis of quasi-static cooling is well

verified; an underlying quiescent coronal emission is not required to obtain a good fit. The best fits are shown by solid lines in Figure 2. From the peak values of T and EM , and the quasi-static radiative time scale, we derived loop parameters as listed in Table 3. The detailed procedure is written in Appendix. The aspect ratio a of 0.07 is within the range for solar active-region loops (0.06 $\leq a \leq 0.2$, Golub et al. 1980), which supports the assumed solar analogy.

4.1.2. Flares II and III

The appearance of Flare II can be interpreted either by the reheating of the plasma cooled during Flare I, or by the heating of a distinct plasma volume, independent from that of Flare I. In the latter case, the lightcurve and EM would be the sum of Flare I component and new arc component. The EM of the new arc component can be derived by subtracting the component extrapolated from Flare I. The derived EM are 1.6 0.4 (phase 4), 2.5 0.8 (phase 5), and 1.9 1.5 (phase 6). Then we fitted the lightcurve and EM with the quasi-static model assuming the above two possibilities. However, in both of the cases, the model did not reproduce the lightcurve and EM simultaneously, and the quasi-static cooling model cannot be adopted throughout the triple arc but Flare I.

For simplicity, we fitted the parameters in Flare II with an exponential model. The best-fit parameters are shown in Table 2, and each models for the reheating and the distinct arc assumptions are shown by the dashed and the dotted lines in Figure 2, respectively. The obtained χ^2_{red} and the timescale for each lightcurve and EM were similar between the two assumptions. Therefore both of the possibilities cannot be discriminated. As for EM , both of the fits show no decay or very long time decay, which is not seen in the usual solar arcs. The constant feature in EM makes the quasi-static model unacceptable.

Since we cannot derive the aspect ratio of Flare II by fitting with quasi-static cooling model, assuming the ratio derived in Flare I and that radiative cooling is dominant, we deduced the plasma parameters as shown in Table 3. Here, we derived the values assuming the reheating scenario (the former assumption). The results show that the plasma density and the volume remain roughly constant from Flare I. This supports that Flare II resulted from reheating of the plasma created by Flare I.

As for Flare III, because of the poor statistics and short observed period, the fits to lightcurve with the exponential model give no constrain between the above two possibilities. The results are shown in Table 2 and Figure 2. We derived the plasma parameters of Flare III in the same way for Flare II, as shown in Table 3. These values are similar to those in Flare I and II. All these are consistent with the scenario that a quasi-periodic reheating makes the triple flare. The heating interval is 20 hour. The loop size is approximately constant through the three flares and is as large as $14 R_{\odot}$. The periodicity and the large-scale magnetic structure support a scenario that an interaction between the star and the disk occurred by the differential rotation and reheated the same loop periodically (e.g., Hayashi, Shibata, & Matsumoto 1996). The detail will be presented in Paper II (Matsumoto et al. 1999).

4.2. Comparison with Other Flares

Among YSOs, TTSs have been known for strong X-ray time variabilities since the Einstein Observatory discovered them (see x1). At any given moment, 5-10% are caught in a high-amplitude flare with timescales of hours (Feigelson & Matsumoto 1999). The most recent example is that of V773 Tau, which exhibits day-long flares with $L_{X,\text{peak}} = 2 \times 10^{32} \text{ erg s}^{-1}$ and very high temperatures of 10^8 K (Tsuboi et al. 1998). Other examples of bright TTS X-ray flares are P1724, a W TTS in Orion ($L_{X,\text{peak}} = 2 \times 10^{33} \text{ erg s}^{-1}$; Preibisch, Neuhauser, & Alcalá 1995), and LkH 92, a CTTS in Taurus (Preibisch, Zinnecker, & Schmitt 1993). These X-ray properties resemble those of RS CVn systems.

Recently, a dozen protostars have been detected in X-rays, and four of those showed evidence for flaring (RCRA core; Koyama et al. 1996, EL29; Kamata et al. 1997, Y LW 15; Grosso et al. 1997, and SSV 63 E+W; Ozawa et al. 1999). In the "super flare" of Y LW 15 (Grosso et al. 1997), an enormous X-ray luminosity was recorded during a few hours. If we adopt the absorption we derived ($N_H = 3 \times 10^{22} \text{ cm}^{-2}$), the absorption-corrected X-ray luminosity in 0.1-100 keV band is $L_{X,\text{peak}} = 10^{34} \text{ erg s}^{-1}$. The "triple flare" we detected in this observation does not reach the same level as the "super flare": $L_{X,\text{peak}} = 5 \times 20 \times 10^{31} \text{ erg s}^{-1}$ in the same X-ray band.

To compare the flare properties of our triple flare from Y LW 15 with other flare sources, including RS CVn systems, we selected bright flare sources as seen in Table 4. All the flare sources have a well-determined temperature using a

wide range of energy band of Tenma; Ginga, and ASCA satellites. Since the samples of YSO flares were less, we added two TTS flares; the flares on ROX s21 and SR 24N detected in our observations (see x2 and x3). We analyzed them using GIS data. The densities and volumes for all the sources were derived assuming that radiative cooling is dominant.

As a result, we found that although less energetic than the "super flare", with total energies in excess of 3.6×10^{36} ergs, the triple flares are on the high end of the energy distribution for protostellar flares. While the plasma densities, temperatures, and then derived equipartition magnetic fields are typical of stellar X-ray flares, the emitting volume is huge; it exceeds those in binary systems of RS CVns by a few orders of magnitude.

5. SUMMARY AND CONCLUSIONS

In the course of a long exposure of the Oph cloud with ASCA, we found evidence for a "triple flare" from the Class I protostar Y LW 15. This triple flare is the first example of its kind; it shows an approximate periodicity of 20 hours. Each event shows a clear decrease in the temperature, followed by reheating, with $kT_{\text{peak}} = 4.6 \text{ keV}$, and luminosity $L_{X,\text{peak}} = 5 \times 20 \times 10^{31} \text{ erg s}^{-1}$. Apart from the periodicity, the characteristics of the flares are among the brightest X-ray detections of Class I protostars.

Fitting with the quasi-static model (VM), which is based on solar flares, reproduces the first flare well, and it suggests that the plasma cools mainly radiatively, having semi-circular shape with length $14 R_{\odot}$ (radius of the circle $R = 4.5 R_{\odot}$) and aspect ratio 0.07. The minimum value of the connecting field is $B = 150 \text{ G}$. The two subsequent flares have weaker intensity than the first one but consistent with the reheating of basically the same magnetic structure as the first flare. The plasma volume is huge; a few orders of magnitude larger than the typical flares in RS CVn systems.

The fact that the X-ray flaring is periodic suggests that the cause for the heating is periodic, hence is linked with rotation in the inner parts of the protostar. The large size of the magnetic structure and the periodicity support the scenario that the flaring episode has originated in a star-disk interaction; differential rotation between the star and disk would amplify and release the magnetic energy in one rotation period or less, reheating the flare loop as observed in the second and third flares.

The authors thank all the members of the ASCA team whose efforts made this observation and data analysis available. We also thank Prof. Eric D. Feigelson, Mr. Kenji Hamaguchi, Dr. Mitsuhiro Hayashi, Dr. Antonio Mazzagatti, Mr. Michael S. Sipior, and Prof. Kazunari Shibata for many useful comments in the course of this work. Y.T. acknowledges the award of Research Fellowship of the Japan Society for Young Scientists.

REFERENCES

Andre, P., & Matsumoto, T. 1994, *ApJ*, 420, 837
 Barsony, M., Kenyon, S. J., Lada, E. A., & Teuben, P. J. 1997, *ApJS*, 112, 109
 Bouvier, J., & Appenzeller, I. 1992, *A & AS*, 92, 481

Burke, B. E., Mountain, R. W., Harrison, D. C., Bautz, M. W., Doty, J. P., Ricker, G. R., & Daniels, P. J. 1991, *IEEE Trans. ED* -38, 1069
 Chen, H., Myers, P. C., Ladd, E. F., & Wood, D. O. S. 1995, *ApJ*, 445, 377

Table 2
Fitting of cooling phase of flares

model expression	F	F _p	ks	χ^2_{red} (d.o.f.)	
[1]	[2]	[3]	[4]	[5]	[6]
$F_{I,\text{qs}}(t) = F_p \cdot f1 + (t - t_1) = g$	I [cntsks ⁻¹]	4	172 5	31 1	0.8 (45)
	kT [keV]	8/7	5.6 0.6	[31]	0.5 (2)
	EM [10^{54} cm^{-3}]	26/7	10.4 0.9	[31]	0.4 (2)
$F_{II}(t) = F_p \cdot \exp(f(t - t_{II})) = g$	I [cntsks ⁻¹]	{	62 3	33 3	1.7 (47)
	kT [keV]	{	4 1	50 20	1.5 (1)
	EM [10^{54} cm^{-3}]	{	3 1	> 53	0.4 (1)
$F_{I+II}(t) = F_{I,\text{qs}}(t) + F_{II}(t)$	I [cntsks ⁻¹]	{	46 3	29 2	1.6 (47)
	EM [10^{54} cm^{-3}]	{	1.6 0.8	> 54	0.6 (1)
$F_{III}(t) = F_p \cdot \exp(f(t - t_{III})) = g$	I [cntsks ⁻¹]	{	35 2	60 20	1.4 (24)
	kT [keV]	{	5 3	55 > 16)	$\chi^2 = 0$ (0)
	EM [10^{54} cm^{-3}]	{	2.5 0.7	71 > 23)	$\chi^2 = 0$ (0)
$F_{I+II+III}(t) = F_{I+II}(t) + F_{III}(t)$	I [cntsks ⁻¹]	{	28 2	60 20	1.4 (24)

Note. | Panel 1 gives the quasi-static t for Flare I. Panel 2 (Panel 3) gives the exponential t for Flare II (Flare III): first assuming that the areas are reheating of the same plasma volume as the previous area; second assuming that the three areas are independent (the previous areas contribute to the latter areas). t_I , t_{II} , and t_{III} are the beginning time of Flare I, II, and III, respectively. We assume only positive values for the decay time (Column [5]). The errors are at 90 % confidence level.

Table 3
Physical parameters for the triple flare

Flare	a	L [R]	n_e [10^{11} cm^{-3}]	B [G]	$L_{X,\text{peak}}$ [$10^{31} \text{ erg s}^{-1}$]	ks	E_{tot} [10^{36} erg]
I	0.07 0.02	14 2	0.5 0.1	150 20	20 1	31 1	6.0 0.5
II	[0.07 0.02]	11 5	0.4 0.1	120 30	8 1	33 3	2.8 0.6
III	[0.07 0.02]	15 10	0.3 0.2	100 60	4.6 0.5	60 20	2.7 1.0

Note. | a: diameter-to-length ratio of the loop; L: loop length; n_e : electron density; B: minimum value of the magnetic field conning the loop plasma; $L_{X,\text{peak}}$: X-ray luminosity at the area peak in the 0.1{100 keV band; : characteristic decay time of the lightcurve; E_{tot} : total energy released during the cooling phase in X-ray wavelength.

Table 4
Comparison with the other flares

Source	SED	n_e [10^{11} cm^{-3}]	V [10^{33} cm^{-3}]	[ks]	kT_{peak} [keV]	$E_{\text{M peak}}$ [10^{55} cm^{-3}]	E_{tot} [10^{36} erg]	ref.
Y LW 15 (I)	I	0.5	3	31	6	0.7	6	
Y LW 15 (II)	I	0.4	2	33	5	0.3	3	
Y LW 15 (III)	I	0.3	2	60	4	0.2	3	
EL29	I	1	0.2	8	4	0.3	0.4	(1)
RC RA	I	1	0.04	20	6	0.04	0.2	(2)
SSV 63E + W	I	1	2	10	6	2	4	(3)
SR24N	II	5	0.1	6	7	3	6	
ROXs31	III	3	0.6	7	6	6	13	
ROX 7	III	3	0.01	6	3	0.1	0.1	(1)
V 773Tau	III	3	0.6	8	10	5	8	(4)
Algol		1	0.09	20	5	0.1	0.6	(5)
Peg		8	0.006	2	6	0.3	0.2	(6)
AU Mic		6	0.002	2	5	0.06	0.03	(7)

Note. | reference: (1) Kamata et al. 1997
 (2) Koyama et al. 1996 and Hamaguchi private comm.
 (3) Oza et al. 1999
 (4) Tsuboi et al. 1998
 (5) Stern et al. 1992
 (6) Doyle et al. 1991
 (7) Cully et al. 1993

Chen, H., Greenfell, T. G., Myers, P. C., & Hughes, J. D. 1997, *ApJ*, 478, 295
 Cully, S. L., Siegmund, O. H. W., Vedder, P. W., & Vallerga, J. V. 1993, *ApJ*, 414, L49
 Dame, T. M. et al. 1987, *ApJ*, 322, 706
 Doyle, J. G. et al. 1991, *MNRAS*, 248, 503
 Feigelson, E. D., & DeCampli, W. M. 1981, *ApJ*, 243, L89
 Feigelson, E. D., & M. Otrnle, T. 1999, *ARA & A*, in press
 Gobub, L., Maxson, C., Rosner, R., Vaiana, G. S., & Serio, S. 1980, *ApJ*, 238, 343
 Gotthelf, E. 1996, *ASCA NEW S* (Greenbelt: NASA GSFC), 4, 31
 Grosso, N., M. Otrnle, T., Feigelson, E. D., Andre, P., Casanova, S., & Gregorio-Hetem, J. 1997, *Nature*, 387, 56
 Hayashi, M. R., Shibata, K., & Matsumoto, R. 1996, *ApJ*, 468, L37
 Ishisaki, Y., Matsuzaki, K., Shirahashi, A., Takahashi, T., & Itoh, R. 1998, Interactive Tool for Data Analysis for DISPLAY 45 (version 1.80)
 Kamata, Y., Koyama, K., Tsuboi, Y., & Yamuchi, S. 1997, *PASJ*, 49, 461
 K nude, J. & Hog, E. 1998, *aap*, 338, 897
 Koyama, K., Maeda, Y., Ozaki, M., Ueno, S., Kamata, Y., Tawara, Y., Skinner, S., & Yamuchi, S. 1994, *PASJ*, 46, L125
 Koyama, K., Hamaguchi, K., Ueno, S., Kobayashi, N., & Feigelson, E. D. 1996, *PASJ*, 48, L87
 Leous, J. A., Feigelson, E. D., Andre, P., & M. Otrnle, T. 1991, *ApJ*, 379, 683
 Makishima, K., et al. 1996, *PASJ*, 48, 171
 M. Otrnle, T., Koch-Miramond, L., Falgarone, E., & Grindlay, J. E. 1983, *ApJ*, 269, 182
 M. Otrnle, T., Grosso, N., Tsuboi, Y., & Koyama, K. 1999, *ApJ*, submitted
 Motte, F., Andre, P., & Neri, R. 1998 *A & A*, 336, 150
 Neuhauser, R., Preibisch, T. 1997 *A & A*, 322, L37
 Ohashi, T., Ebisawa, K., Fukazawa, Y., Hayashi, K., et al. 1996, *PASJ*, 48, 157
 Oza, H., Nagase, F., Ueda, Y., Dotani, T., & Ishida, M. 1999, *ApJ*, 523, L81
 Preibisch, T., Zinnecker, H., & Schmitt, J. H. M. M. 1993, *A & A*, 279, L33
 Preibisch, T., Neuhauser, R., & Alcal, J. M. 1995, *A & A*, 304, L13
 van den Oord, G. H. J. & Mewe, R. 1989, *A & A*, 213, 245
 Serlemitsos, P. J., et al. 1995, *PASJ*, 47, 105
 Shu, F. H., Adams, F. C., & Lizano, S. 1987, *ARA & A*, 25, 23
 Stelzer, B., Neuhauser, R., Casanova, S., & M. Otrnle, T. 1999, *A & A*, 344, 154
 Stern, R. A., Uchida, Y., Tsuneta, S., & Nagase, F. 1992, *ApJ*, 400, 321
 Tanaka, Y., Inoue, H., & Holt, S. S. 1994, *PASJ*, 46, L37
 Tsuboi, Y., Koyama, K., Murakami, H., Hayashi, M., Skinner, S., Ueno, S. *ApJ*, 503, 894
 Wilking, B. A., & Lada, C. J. 1983, *ApJ*, 274, 698

APPENDIX

DETERMINATION OF THE PHYSICAL PARAMETERS OF THE FLARES

1. LOOP PARAMETERS

We make use of the general treatment for solar-type flares, put forward by van den Oord & Mewe (1989, hereafter VM). The decrease in the thermal energy of the cooling plasma is assumed to be caused by radiative (r) and conductive losses (c): its decay time is thus $1 = e^{-1} = 1 = r + 1 = c$. VM assumed that the flare lightcurve and temperature decrease exponentially with decay times d and T , respectively. This effective cooling time is related to observed time scales by $1 = e^{-1} = 7 = 8 T + 1 = 2 d$. We assume here that the flare occurs in only one semi-circular loop with constant section along the tube flux, radius R ($R = L$; length L), diameter-to-length ratio a , and volume V . VM gives an expression of L versus a , depending on e , the temperature, the emission measure (hereafter EM), and the ratio $r = c$. Because of the assumed exponential behavior of the lightcurve and temperature, the moment at which this expression is applied is not important. The only restriction is that both the temperature and the EM started to decrease.

Due to the low statistics, we have only time-sliced values of the temperature and the EM. Let us call t_i (t_f) the beginning (end) of the time interval within which the temperature was estimated, we have: $\bar{T} = \frac{R_{t_f}}{t_f - t_i} \int_{t_i}^{t_f} T(t) dt = (t_f - t_i)$. We use this relation to find the behavior of the temperature as a function of time.

We now have a relation between L and a , but the ratio $r = c$ is unknown, and even worse may change during the decay of the flare. An exception to this is when the flare volume cools quasi-statically, evolving through a sequence of quasi-static equilibria, where the loop satisfies scaling laws, and where $r = c = \text{cst}$. Due to the dependency of r and c on the temperature and the EM, $r = c = \text{cst}$ implies $T^{13/4} = \text{EM} = \text{cst}$. VM gives in that case analytical expressions for several physical quantities versus time, all depending on the quasi-static radiative time scale (r_{qs}). r_{qs} can be estimated from the lightcurve which must be proportional to the radiative loss. The temperature and the EM can be fitted as described above using this value of r_{qs} , and give the peak values $kT_{p,qs}$, $\text{EM}_{p,qs}$ (see Col. 4]{5} in our Table 2, panel 1 for details).

Using an expression for the radiative time (eq. [23a] of VM), the EM (eq. [3] of VM) and the scaling law (SL 2], eq. [196] of VM), we obtained the loop characteristics for the quasi-static model:

$$a = 1.38 \quad (r_{qs}=10 \text{ ks})^{1/2} \quad (kT_{p,qs}=\text{keV})^{33/16} \quad (\text{EM}_{p,qs}=10^{54} \text{ cm}^{-3})^{1/2}; \quad (1)$$

$$L = 1.0 R \quad (r_{qs}=10 \text{ ks}) \quad (kT_{p,qs}=\text{keV})^{7/8}; \quad (2)$$

$$n_e = 4.4 \quad 10^{10} \text{ cm}^{-3} \quad (r_{qs}=10 \text{ ks})^{1/4} \quad (kT_{p,qs}=\text{keV})^{3/4}; \quad (3)$$

Using an expression for the ratio $r = c$ on page 252 of VM, we found $r = c = f$, with the parameter depending only on the exponent of the temperature in the expression for the radiative loss (for temperature above 20 MK, $f = 0.18$), and the multiplicative function f coming from the expression for the mean conductive energy loss (formula [7] of VM), which is equal to 4/7 for a loop with a constant section. Thus, $r = c = 0.1 \cdot 0.18^{3/4} = 0.1$.³ In other words, the quasi-static model implies that 91% of the lost energy are radiative losses: radiation is the dominant energy loss process.

Assuming that the cooling is only radiative we used these simplified relations based on the exponential decay of the lightcurve, the temperature, and the EM:

$$n_e = 4.4 \quad 10^{10} \text{ cm}^{-3} \quad (d=10 \text{ ks})^{1/4} \quad (kT_p=\text{keV})^{3/4}; \quad \text{for } kT > 2 \text{ keV}; \quad (4)$$

$$L = 7.4 R \quad (a=0.07)^{2/3} \quad (d=10 \text{ ks})^{2/3} \quad (kT_p=\text{keV})^{1/2} \quad (\text{EM}_p=10^{54})^{1/3}; \quad (5)$$

with kT_p (EM_p) the peak value of the temperature (EM).

2. MAGNETIC FIELD

Assuming equipartition between the magnetic pressure $B^2/8\pi$ and the ionized gas pressure $2n_e kT$, we can obtain a minimum value of the magnetic field connecting the emitting plasma using:

$$B = 28.4 G \quad (n_e=10^{10} \text{ cm}^{-3})^{1/2} \quad (kT=\text{keV})^{1/2} \quad (6)$$

3. RELEASED ENERGY

For estimating the energy released by the flare during its cooling phase we need the peak luminosity value of this flare. As the lightcurve must be proportional to the intrinsic luminosity, we fit the time averaged intrinsic luminosities in the 0.1{100 keV band (given in Table 1) with the same model used for the lightcurve fitting. This gives the peak luminosity, $L_{x,peak}$, and a characteristic decay time τ . Thus, the total energy released by this flare is:

$$E_{\text{tot}} = 10^{35} \text{ erg} \quad (L_{x,peak}=10^{32} \text{ erg s}^{-1}) \quad (\tau=10 \text{ ks}) \quad (7)$$

³VM wrote $r = c = 0.18$, and the analytical expression for the conductive energy loss in the quasi-static model without taking this multiplicative factor 4/7 into account (see Table 5 of VM).